The Astrophysical Journal, 857:107 (11pp), 2018 April 20 https://doi.org/10.3847/1538-4357/aab712

A Short-term ESPERTA-based Forecast Tool for Moderate-to-extreme Solar Proton Events

M. Laurenza[1], T. Alberti[1,2], and E. W. Cliver[3,4]
[1] INAF-IAPS, Via del Fosso del Cavaliere, 100, I-00133, Roma, Italy; monica.laurenza@iaps.inaf.it
[2] Dipartimento di Fisica, Università della Calabria, Ponte P. Bucci, Cubo 31C, I-87036, Rende (CS), Italy
[3] National Solar Observatory, 3665 Discovery Drive, Boulder, CO 80303, USA
[4] Air Force Research Laboratory, Space Vehicles Directorate, 3550 Aberdeen Ave., Kirtland AFB, NM 87117, USA
Received 2017 December 4; revised 2018 March 5; accepted 2018 March 9; published 2018 April 20

Abstract

The ESPERTA (Empirical model for Solar Proton Event Real Time Alert) forecast tool has a Probability of Detection (POD) of 63% for all >10 MeV events with proton peak intensity ⩾10 pfu (i.e., ⩾S1 events, S1 referring to minor storms on the NOAA Solar Radiation Storms scale), from 1995 to 2014 with a false alarm rate (FAR) of 38% and a median (minimum) warning time (WT) of ∼4.8 (0.4) hr. The NOAA space weather scale includes four additional categories: moderate (S2), strong (S3), severe (S4), and extreme (S5). As S1 events have only minor impacts on HF radio propagation in the polar regions, the effective threshold for significant space radiation effects appears to be the S2 level (100 pfu), above which both biological and space operation impacts are observed along with increased effects on HF propagation in the polar regions. We modified the ESPERTA model to predict ⩾S2 events and obtained a POD of 75% (41/55) and an FAR of 24% (13/54) for the 1995–2014 interval with a median (minimum) WT of ∼1.7 (0.2) hr based on predictions made at the time of the S1 threshold crossing. The improved performance of ESPERTA for ⩾S2 events is a reflection of the big flare syndrome, which postulates that the measures of the various manifestations of eruptive solar flares increase as one considers increasingly larger events.

Key words: methods: data analysis – Sun: activity – Sun: flares – Sun: particle emission – Sun: radio radiation – Sun: X-rays, gamma rays

1. Introduction

Accurately predicting solar activity is notoriously difficult, be it on solar cycle or short-term (hours) timescales (e.g., Pesnell 2012; Barnes et al. 2016). The ultimate test of our understanding of solar activity will be to reliably predict, in advance of their occurence on the Sun, the timing of solar eruptions and the severity of their terrestrial impacts. Such expertise lies in the future. More promising now are techniques that exploit the disturbance propagation delay between eruptive flares and their magnetic or proton impacts at 1 au. The chief hurdle for accurate predictions of geomagnetic storms using this approach is the difficulty of determining the orientation of the magnetic field of the responsible coronal mass ejection (CME), although progress is being made on this front (e.g., Marubashi et al. 2015). For solar proton events (SPEs), the primary obstacle for the reliable warning of impending events is the rapid and reliable determination of the CME speed and the identification of shock formation (the principal determinants of the acceleration of energetic protons observed in space Reames 1999, 2013, 2017; Cliver 2016), given that the lowest energy protons of interest (∼10 MeV) propagate to Earth in ∼1 hr.

During the last decade, with increasing focus on the applied (or space weather) aspects of solar–terrestrial physics (US National Academy of Sciences[5] 2008; Lloyds[6] of London 2010; JASON[7] 2011; and the UK Royal Academy of Engineering[8] 2013, among others), a number of methods (e.g., Kahler et al. 2007; Posner 2007; Balch 2008; Laurenza et al. 2009; Núñez 2011; Papaioannou et al. 2015; Winter & Ledbetter 2015; Alberti et al. 2017; St. Cyr et al. 2017) have been investigated to provide advance warning of SPEs with intensities ⩾10 proton flux units (pfu; 1 pfu = 1 pr cm^{-2} s^{-1} sr^{-1}). Such SPEs are designated "minor" (or S1) events on the NOAA Space Weather Prediction Center (SWPC) scale of Solar Radiation Storms (Table 1; http://www.swpc.noaa.gov/noaa-scales-explanation). The utility of such forecasts is quantified using categorical scores of forecasting parameters (e.g., Balch 2008). Crucial metrics include the percentage of the SPE events that are correctly predicted (Probability of Detection—POD), the percentage of those that are erroneously identified as events (False Alarm Rate—FAR), and the lead warning time (WT). Alberti et al. (2017) recently validated the ESPERTA (Empirical model for Solar Proton Event Real Time Alert, Laurenza et al. (2009; see also Laurenza et al. 2007; Storini et al. 2008; Signoretti et al. 2011) proton prediction tool by using an independent data set for the interval from 2006 to 2014, outside of the 1995 to 2005 period for which ESPERTA was developed. The ESPERTA prediction parameters they obtained for this interval are fairly typical for such SPE forecast methods (see Table 1 in Anastasiadis et al. 2017): POD = 59% (19/32); FAR = 30% (8/27); median (minimum) warning time = ∼2 (0.4) hr (range from 0.4 to 35.9 hr) and are similar to those determined by Laurenza et al. (2009) for the 1995–2005 development period.

A prime focus of the ESPERTA model was to provide timely warnings, within 10 minutes of the flare soft X-ray (SXR) maximum. Within this time constraint, it is difficult to confidently determine CME speeds and identify the radio type II bursts that signal the existence of coronal shocks. Thus ESPERTA is based on input flare data (flare location, flare 1–8 Å SXR fluence, and flare 1 MHz radio fluence) that are, or

[5] National Academy of Sciences: https://www.nap.edu/catalog/12507/severe-space-weather-events-understanding-societal-and-economic-impacts-a.
[6] Lloyds: http://www.lloyds.com/~/media/lloyds/reports/360/360%20space%20weather/7311_lloyds_360_space%20weather_03.pdf.
[7] JASON: https://fas.org/irp/agency/dod/jason/spaceweather.pdf.
[8] Royal Academy: http://www.raeng.org.uk/publications/reports/space-weather-full-report.

Table 1
NOAA Space Weather Scales (Adapted from http://www.swpc.noaa.gov/noaa-scales-explanation)

Solar Radiation Storms			Flux Level of ⩾10 Mev Particles (ions)	Number of Events when Flux Level was met
S5	Extreme	Biological: unavoidable high radiation hazard to astronauts on EVA (extra-vehicular activity); passengers and crew in high-flying aircraft at high latitudes may be exposed to radiation risk. Satellite operations: satellites may be rendered useless, memory impacts can cause loss of control, may cause serious noise in image data, star-trackers may be unable to locate sources; permanent damage to solar panels possible. Other systems: complete blackout of HF (high frequency) communications possible through the polar regions, and position errors make navigation operations extremely difficult.	10^5	Fewer than 1 per cycle
S4	Severe	Biological: unavoidable radiation hazard to astronauts on EVA; passengers and crew in high-flying aircraft at high latitudes may be exposed to radiation risk. Satellite operations: may experience memory device problems and noise on imaging systems; star-trackers problems may cause orientation problems, and solar panel efficiency can be degraded. Other systems: blackout of HF radio communications through the polar regions, and increased navigation errors over several days are likely.	10^4	3 per cycle
S3	Strong	Biological: radiation hazard avoidance recommended for astronauts on EVA; passengers and crew in high-flying aircraft at high latitudes may be exposed to radiation risk. Satellite operations: single-event upsets, noise in imaging systems, and slight reduction of efficiency in solar panel are likely. Other systems: degraded HF radio propagation through the polar regions and navigation position errors likely.	10^3	10 per cycle
S2	Moderate	Biological: passengers and crew in high-flying aircraft at high latitudes may be exposed to elevated radiation risk. Satellite operations: infrequent single-event upsets possible. Other systems: effects on HF propagation through the polar regions, and navigation at polar cap locations possibly affected.	10^2	25 per cycle
S1	Minor	Biological: none Satellite operations: none. Other systems: minor impacts on HF radio in the polar regions.	10	50 per cycle

could be made, available in real time. These three parameters provide information on proton propagation, solar event energy, and particle escape, respectively. ESPERTA forecasts are only made for SXR flares of ⩾M2 class (peak intensity $\geqslant 2 \times 10^{-5}\,\mathrm{W\,m^{-2}}$). Table 1 shows that SWPC has four additional warning levels for proton storms beyond the S1 (minor) proton event classication. These are S2 (moderate; 10^2 pfu), S3 (strong; 10^3 pfu), S4 (severe; 10^4 pfu), and S5 (extreme; 10^5 pfu). The listed effects for S1 events are relatively benign. Only at the S2 level are biological and satellite operation effects sensible, in addition to increased (over S1) HF propagation effects in the polar regions. A few operational forecasting tools currently provide alerts of SPEs together with a quantification of their expected terrestrial impact (COMESEP SEP Forecasting tool, Dierckxsens et al. 2015; the FORSPEF tool, Papaioannou et al. 2015; NOAA Space Weather Alerts and Warnings), although they have not been validated in terms of the predicted peak flux. In this study, we will evaluate the ESPERTA model for ⩾S2 SPEs, which are an order of magnitude, or more, larger than the smallest S1 events. Our list of ⩾S2 events with flare, CME, and coronal shock associations for the 1995–2015 interval analysis is presented in Section 2, the ESPERTA-based S2 event forecasting technique is developed in Section 3 and the results are summarized and discussed in Section 4.

2. Database

We compiled a list of ⩾S2 SPEs from 1995 to 2014 by beginning with the published lists of ⩾S1 events from Laurenza et al. (2009) and Alberti et al. (2017) for 1995–2005 and 2006–2014, respectively. As a second step, we surveyed 5 minute averaged proton data (https://satdat.ngdc.noaa.gov/sem/goes/data/avg/) obtained from the particle instruments on board the *Geostationary Operational Environmental Satellite* (*GOES*) spacecraft series during their

operational time: the energetic particle sensor (EPS) instrument on board GOES 8–12 and the Energetic Proton, Electron and Alpha Detector (EPEAD) on GOES 13 and 15. We used the satellite with the highest peak >10 MeV flux for each SPE. As is the case for the identification of ⩾S1 events, we required that ⩾S2 events meet or exceed the S2 (100 pfu) threshold for three consecutive 5 minute averaging intervals, which correspond to three data points. Of the 129 ⩾ S1 events identified by Laurenza et al. (2009) and Alberti et al. (2017), about half (59) were ⩾S2 events. The 59 ⩾ S2 events do not include two events (2003 October 29 and 2005 January 17) for which a factor of two increase in >10 MeV intensity was predicted above a ⩾100 pfu background. They do include an SPE on 2006 December 14 that was mistakenly classified as an FA in Alberti et al. (2017), a shock spike event on 2004 September 12 (see Section 3.2), and an SPE on 2002 August 24 that was not considered in Laurenza et al. (2009) because of a minor data gap in the radio data (too small to keep this event outside of the probability threshold contour (see Section 3.1); the data gap was not filled and the fluence was computed over the remaining points in the interval).

In Table 2, we list flare, CME, and forecast data for each of these 59 events in the following columns: (1) event number, (2) flare date, (3) peak time of the SXR burst, (4) SXR burst class (based on the *GOES* peak 1–8 Å intensity as follows: classes C1-9, M1-9, and X1-9 correspond to flare peak intensities of (1–9) × 10^{-6}, (1–9) × 10^{-5}, and (1–9)×10^{-4} W m^{-2}, respectively), (5) heliographic location of the associated solar eruption, (6) time-integrated SXR intensity (http://spidr.ionosonde.net/spidr/index.jsp), (7) SXR integration flag (see Laurenza et al. 2009 and Alberti et al. 2017 for the determination of both SXR (column 6) and radio (column 8) fluences), (8) time-integrated ∼1 MHz *Wind*/Waves type III intensity (ftp://solar-radio.gsfc.nasa.gov/; Bougeret et al. 1995), (9) actual (closest to 1 MHz) frequency used in column (8), (10) linear CME speed from *SOHO*/LASCO catalog (Yashiro et al. 2004; Gopalswamy et al. 2009); D.G. = data gap, (11) SWPC radiation class, (12) WT for ⩾S2 events, difference between S2 threshold crossing time (end of three consecutive 5 minute intervals with >10 MeV flux ⩾100 pfu) and the S1 threshold crossing time (end of three consecutive 5 minute intervals with >10 MeV flux ⩾10 pfu). For events in Column (12) that are flagged by **, the listed WT is the difference between the S2 crossing time and the flare SXR peak time plus 10 minutes. The SPE identifications and flare associations are consistent with those of Cane et al. (2010), Richardson et al. (2014), and (I. G. Richardson 2017, private communication). Column (13) reports the SPE forecast result (where "Hit," "Miss," "MISS," and "blank" refer to SPEs correctly predicted (41 cases), SPEs with associated front-side or far-side ⩾M2 SXR flares that were not predicted (8 cases), SPEs with associated front-side <M2 SXR flares (6 cases; no prediction made), and SPEs associated with backside flares with SXR peaks <M2 (4 cases; not included in the forecast statistics)). Figure 1 gives plots of the >10 MeV SPE time profiles (highest *GOES* data) for each of the 41 S2 "Hit" events in Table 2. The vertical red line gives the time 10 minutes after the peak of the ⩾M2 SXR flare (when S1 alerts are issued), the light blue line gives the time that the proton event intensity crossed the S1 level (i.e., the end of the third consecutive 5 minute interval with intensity ⩾10 pfu, which is the time that S2 alerts are generally issued (see Section 3.2)), and the black line gives the crossing time of the S2 event threshold (end of the third consecutive 5 minute interval with intensity ⩾100 pfu).

3. Forecasting ⩾S1 and ⩾S2 Events (1995–2014)

3.1. ESPERTA Applied to ⩾S1 (⩾10 pfu) Events

From 1995 to 2014, 980 ⩾ M2 SXR flares were observed. Scatter plots of the ∼1 MHz radio fluence for these flares versus their SXR fluence (both as determined by ESPERTA algorithms from data streams ending within 10 minutes after the 1–8 Å peak Laurenza et al. 2009; Alberti et al. 2017) for three solar longitude ranges are given in Figure 2. The value of the probability assigned to the dashed-line contours for each of the three longitude ranges is based on the logistic regression analysis of McCullagh & Nelder (1983; see also Garcia 1994; Silverman 1998; Laurenza et al. 2009; Alberti et al. 2017). It allows one to compute the probability that an event will occur by using the parametric space with two variables (SXR fluence and radio fluence) for the ⩾M2 SXR flares. The probability (P) can be expressed as

$$P(\log X, \log R) = \frac{e^{\eta}}{1 + e^{\eta}}, \quad (1)$$

where $\eta = \eta(\log X, \log R)$. In the ESPERTA model, the dependence of the probability on the heliographic longitude was taken into account by separating the ⩾M2 flares into three different longitude bands: E 120°–E 41°; E 40°–W 19°; W 20°–W 120°. Thus, three different values for η corresponding to the three longitudinal bands were obtained (Laurenza et al. 2009; Alberti et al. 2017):

1. $\eta_1 = -6.07 - 1.75\log(X) + 1.14\log(R) + 0.56\log(X)\log(R)$.
2. $\eta_2 = -7.44 - 2.99\log(X) + 1.21\log(R) + 0.69\log(X)\log(R)$.
3. $\eta_3 = -5.02 - 1.74\log(X) + 0.64\log(R) + 0.40\log(X)\log(R.)$

Specific values from 0 to 1 for the probability can be assigned in the logistic regression formula with some step that would lead to several contours in each graph of Figure 2 (not plotted; see Figure 6 in Alberti et al. 2017). Then, one probability threshold (PT) contour can be selected above which these probabilistic forecasts are translated into a yes or no warning for an SEP event occurrence: given a ⩾M2 solar flare, if the related data point is above the selected PT contour level, a warning is given; if it is below, none is issued. In the scatter plots of Figure 2 of the radio fluence versus the SXR fluence, a probability of SEP occurrence is obtained for each pair of SXR and radio fluence values. The PT contours (dashed lines in the three scatter plots) in Figure 2 separate SXR events for which a positive forecast of a ⩾S1 event was made (events above the contour) from those for which a null event forecast was made (events below the contour). The probability curve level PT is 28%, 28%, and 23% for western, intermediate, and eastern events, respectively, which is selected to maximize the POD while minimizing the FAR for ESPERTA forecasts over the specified longitude range for this 20-year time interval. The three longitude bins contain a total of 88 colored symbols: 68

Table 2
⩾100 pfu SPE Flare List (1995–2014)

Event Number	SXR Date	SXR Peak Time (hh:mm)	SXR Class	Hα Location	SXR Fluence ($J\ m^{-2}$)	SXR Flag	Radio Fluence (sfu × min)	Radio Frequency (kHz)	CME Linear Speed ($km\ s^{-1}$)	SWPC Radiation Class	S2 Warning Time (minutes)	SPE Forecast Result
1	1997 Nov 6	11:55	X9	S18W63	3.61e–1	7	1.87e+7	940	1556	S2	135	Hit
2	1998 Apr 20	10:21	M1	W115	…	…	…	…	1863	S3	…	…
3	1998 May 2	13:42	X1	S15W15	7.37e–2	5	2.14e+7	940	938	S2	80	Hit
4	1998 May 6	08:09	X2	S11W65	2.35e–1	5	8.85e+6	940	1099	S2	45	Hit
5	1998 Aug 24	22:12	X1	N35E09	1.88e–1	5	1.79e+7	940	D.G.	S2	130	Hit
6	1998 Sep 30	13:48	M3	N23W81	9.61e–2	2	7.09e+5	940	D.G.	S3		Miss
7	1998 Nov 14	05:18	C2	W130	…	…	…	…	D.G.	S2	…	…
8	2000 Jul 14	10:23	X6	N22W07	1.35e+0	5	1.20e+7	940	1674	S4	25	Hit
9	2000 Sep 12	12:12	M1	S19W08	2.94e–2	1	5.43e+6	940	1550	S2		MISS
10	2000 Nov 8	23:37	M8	N10W77	3.36e–1	3	4.51e+6	940	1738	S4	10	Hit
11	2000 Nov 25	01:31	M8	N07E50	2.66e–1	5	1.69e+6	940	2519	S2		Miss
12	2001 Apr 2	21:50	X18	N18W82	1.62e+0	5	2.75e+6	940	2505	S3	90	Hit
13	2001 Apr 10	05:26	X2	S23W09	3.66e–1	5	9.50e+6	940	2411	S2	480	Hit
14	2001 Apr 15	13:50	X16	S20W85	6.20e–1	7	8.77e+6	940	1199	S2	15	Hit
15	2001 Apr 18	02:14	C2	W120	…	…	…	…	2465	S2	…	…
16	2001 Aug 15	23:55	<C1	W180	…	…		…	1575	S2	…	…
17	2001 Sep 24	10:35	X3	S12E29	1.09e+0	3	1.48e+6	940	2402	S4	60	Hit
18	2001 Oct 1	05:15	M9	S22W85	7.56e–2	5	1.12e+5	940	1405	S3		Miss
19	2001 Nov 4	16:19	X1	N07W19	2.76e–1	2	1.36e+7	940	1810	S4	20	Hit
20	2001 Nov 22	23:27	X1	S15W34	4.68e–1	3	1.38e+5	940	1437	S4	163**	Hit
21	2001 Dec 26	05:36	M7	N08W54	6.30e–1	4	1.14e+6	940	1446	S2	30	Hit
22	2001 Dec 28	20:42	X3	S26E95	2.92e+0	4	4.43e+6	940	2216	S2	540	Hit
23	2002 Apr 21	01:47	X1	S14W84	7.82e–1	3	4.51e+6	940	2393	S3	10	Hit
24	2002 May 22	03:48	C5	S22W53	1.82e–2	1	2.02e+6	940	1557	S2		MISS
25	2002 Jul 15	20:08	X3	N19W01	1.49e–1	7	9.81e+6	940	1151	S2	1510	Hit
26	2002 Aug 24	01:11	X3	S02W81	5.75e–1	5	7.83e+5	940	1913	S2	60	Hit
27	2002 Sep 5	17:04	C5	N09E28	2.49e–2	3	2.34e+5	940	1748	S2	…	MISS
28	2002 Nov 9	13:23	M5	S12W29	5.52e–2	5	8.14e+6	940	1838	S2	…	Miss
29	2003 May 29	01:05	X1	S07W38	7.34e–2	5	1.30e+7	940	1366	S2	850**	Hit
30	2003 Oct 26	18:11	X1	N02W38	3.83e–1	1	1.43e+6	916	1537	S2	25	Hit
31	2003 Oct 28	11:10	X18	S16E07	1.96e+0	5	2.16e+7	916	1057	S4	30	Hit
32	2003 Nov 2	17:25	X9	S14W56	1.09e+0	5	2.70e+6	916	2036	S3	55**	Hit
33	2003 Nov 4	19:44	X18	S19W83	2.65e+0	1	9.53e+5	916	2657	S2	430	Hit
34	2004 Jul 25	15:15	M1	N08W33	3.25e–2	1	7.51e+4	940	1233	S3	…	MISS
35	2004 Sep 12	00:56	M5	N04E42	1.64e–1	2	1.16e+7	940	1328	S2	…	Miss
36	2004 Nov 7	16:06	X2	N09W17	2.08e–1	5	1.36e+6	940	1759	S2	100	Hit
37	2004 Nov 10	02:13	X3	N09W49	1.68e–1	7	1.84e+6	940	3387	S2	227**	Hit
38	2005 Jan 15	23:00	X3	N14W08	8.63e–1	2	1.01E+6	916	2861	S2	700	Hit
39	2005 Jan 20	07:00	X8	N12W58	1.97e+0	5	1.66e+7	916	882	S3	50	Hit
40	2005 May 13	16:57	M8	N12E11	2.50e–1	5	1.79e+7	916	1689	S3	930	Hit
41	2005 Jul 14	10:54	X1	W95	6.63e–1	3	2.65e+4	916	1423	S2	…	Miss
42	2005 Aug 22	17:28	M6	S12W60	2.87e–1	3	1.54e+6	916	2378	S2	415	Hit
43	2005 Sep 07	17:40	X18	S06E89	6.65e+0	3	1.42e+7	916	2257	S3	1950	Hit
44	2005 Sep 13	20:04	X1	S09E05	4.86e–1	5	1.49e+5	916	1866	S2	…	Miss
45	2006 Dec 5	10:35	X9	S07E79	6.12e–1	5	1.90e+6	916	D.G.	S3	1150	Hit
46	2006 Dec 13	02:39	X3	S05W23	5.88e–1	5	1.82e+7	916	1774	S2	75	Hit

Table 2
(Continued)

Event Number	SXR Date	SXR Peak Time (hh:mm)	SXR Class	Hα Location	SXR Fluence (J m^{-2})	SXR Flag	Radio Fluence (sfu × min)	Radio Frequency (kHz)	CME Linear Speed (km s^{-1})	SWPC Radiation Class	S2 Warning Time (minutes)	SPE Forecast Result
47	2006 Dec 14	22:15	X1	S06W31	1.36e–1	5	7.52e+6	916	1042	S2	95**	Hit
48	2012 Jan 23	03:59	M8	N28W36	3.97e–2	5	5.26e+5	916	2175	S3	⋯	Miss
49	2012 Jan 27	18:37	X1	N27W71	2.33e–1	5	4.38e+6	916	2508	S2	75	Hit
50	2012 Mar 7	00:24	X5	N17E15	6.89e–1	5	2.19e+7	916	2684	S3	340	Hit
51	2012 Mar 13	17:41	M7	N18W62	2.65e–1	3	2.92e+6	916	1884	S2	75	Hit
52	2012 May 17	01:47	M5	N12W89	1.21e–1	5	9.08e+6	916	1582	S2	75	Hit
53	2012 Jul 17	17:15	M1	S17W75	1.86e–1	⋯	3.27e+5	916	958	S2	⋯	MISS
54	2013 Apr 11	07:16	M6	N09E12	7.11e–2	5	3.38e+7	916	986	S2	295	Hit
55	2013 May 22	13:32	M5	N15W70	1.77e–1	3	5.74e+5	916	1537	S3	330	Hit
56	2013 Sep 29	23:37	C1	N15W40	3.07e–3		6.94e+4	916	1025	S2	⋯	MISS
57	2014 Jan 7	18:32	X1	S15W11	2.95e–1	5	7.85e+6	916	1830	S3	343**	Hit
58	2014 Feb 25	00:49	X4	S12E82	4.64e–1	5	6.83e+6	916	2147	S2	3890	Hit
59	2014 Sep 10	17:45	X1	N16W06	3.88e–1	5	3.49e+7	916	1425	S2	2180	Hit

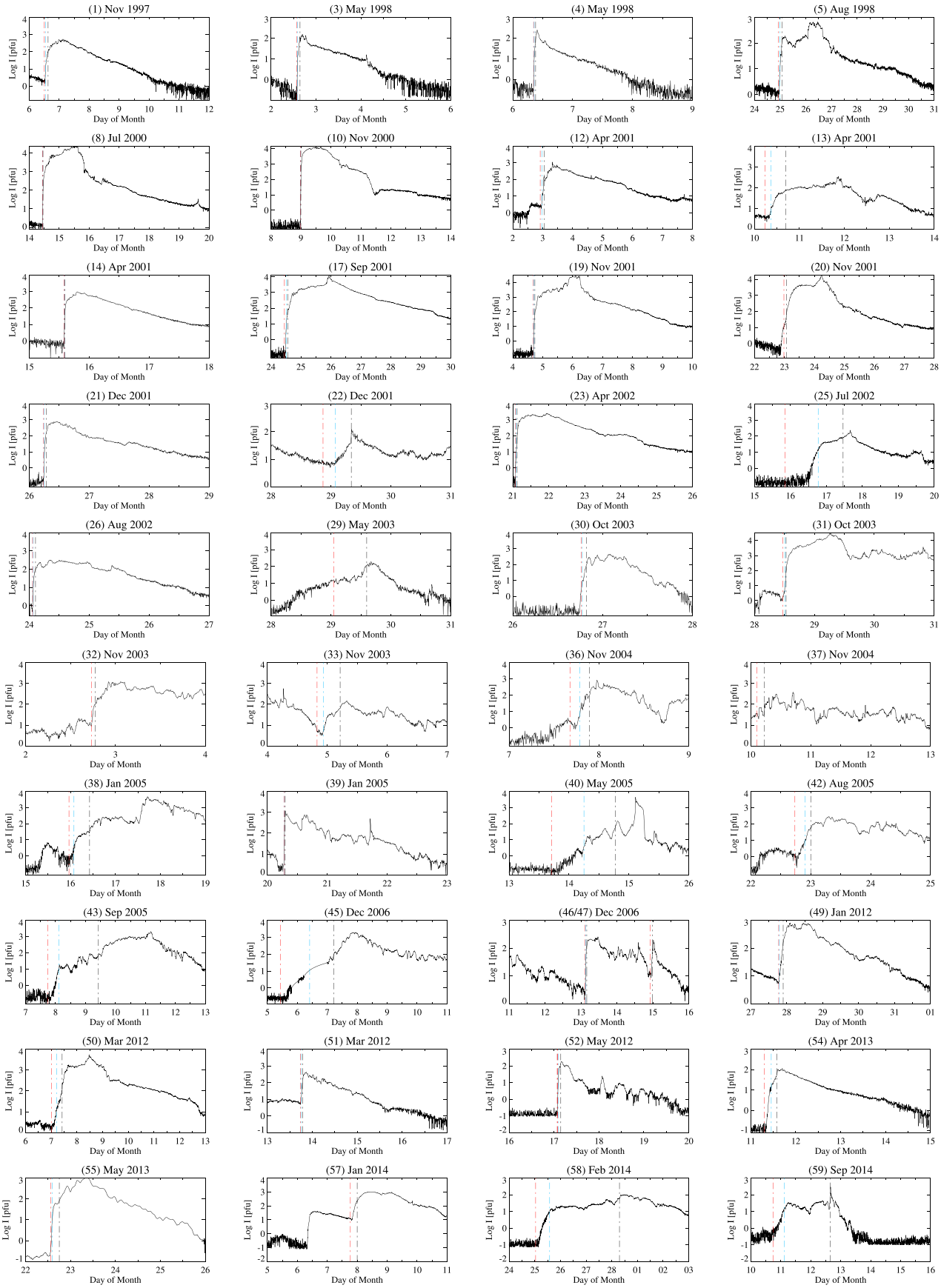

Figure 1. Intensity time profiles for the 41 "Hit" (correctly predicted) $\geqslant$S2 $>$ 10 MeV proton events in Table 2. The vertical red line gives the time 10 minutes after the peak of the $\geqslant$M2 SXR flare, the light blue line gives the time that the proton event intensity crossed the S1 level, and the black line gives the crossing time of the S2 event threshold. The interpolations in the SPE trace for event No. 45 were included in the *GOES* data. Note that event Nos. 46 and 47 are shown in one plot.

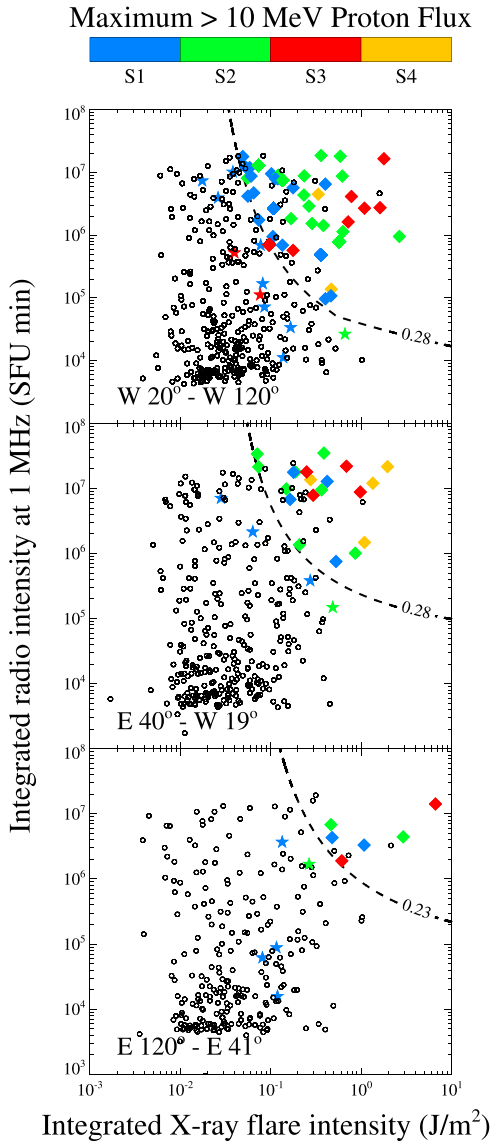

Figure 2. ESPERTA probability contours for the prediction of ⩾S1 SPEs for three solar longitude bands (Laurenza et al. 2007; Alberti et al. 2017). Symbols: open circles outside contours—correct null forecasts; open circles inside contours—false alarms; stars—⩾S1 SPEs not predicted (Misses); diamonds—correctly predicted ⩾S1 SPEs (Hits); ⩾S1 SPEs not preceded by ⩾M2 flares—MISSES (not plotted). Color coding gives the NOAA Radiation Storms scale (Table 1).

diamonds (Hits) and 20 stars ("Misses"; 21 MISSes associated with front-side <M2 flares, not plotted). The color code given at the top of the figure distinguishes the S1-S4 SPEs (there were no S5 events in the sample). Open circles below the PT contour indicate correct null forecasts, while those above indicate FAs. The forecast statistics for the 20-year interval are in good agreement[9] with the POD (62%) and FAR (39%) values obtained by Alberti et al. (2017):

1. POD = Hits/(Hits + Misses + MISSES) = 69/(69+20+21) = 63%.
2. FAR = FAs/(Hits + FAs) = 42/(69+42) = 38%.

For ⩾S1 events, the SPE alert is issued 10 minutes after the ⩾M2 SXR peak and the SPE onset is the end of the third consecutive 5 minute interval for which the average >10 MeV flux is ⩾10 pfu (or when the flux increases by a factor of two for cases where the preflare >10 MeV flux was >10 pfu). The difference between these two times is the forecast WT. The median WT for the hits in our sample of ⩾S1 events for this 20-year interval was 4.8 hr with a range from 0.4 to 52.8 hr Alberti et al. (2017).

3.2. ESPERTA Applied to ⩾S2 (⩾100 pfu) Events

It can be seen in Figure 2 that the majority of S1 events (blue symbols) correspond to relatively low values of SXR and radio fluence. Many of them are Misses (blue stars, 15/38) in ESPERTA. On the contrary, the majority of ⩾S2 SPEs (green, red, and yellow symbols) have high values of SXR and radio fluence, with few Misses (green, red, and yellow stars, 5/47). Thus, if we use ESPERTA to predict ⩾S2 events, we can eliminate 15 events that are not predicted ("Missed" events; blue stars in Figure 2). These 15 events now become correct null forecasts (open circles below the probability contours in Figure 3). Moreover, predicting ⩾S2 events allows us to eliminate 15 of 21 "MISSed" S1 events (not plotted in Figure 2) associated with ⩽M2 SXR flares. These 15 MISSed events are examples of difficult-to-predict ⩾S1 SPEs associated with "proton flares with weak impulsive phases" Cliver et al. (1983).

Modifications to ESPERTA can enhance its performance for predicting ⩾S2 events as shown in Figure 3. First, the ESPERTA probability threshold contours are optimized for forecasting such events for the three longitude ranges. The PT contour for the W20–W120 longitude bin is adjusted upward from a parameter value of 0.28 to 0.35, while the PT contours for the other two bins are left unchanged from those used in Alberti et al. (2017). This results in (1) the conversion of 12 hits (blue diamonds, the S1 events whose data points are located between the 0.28 and 0.35 contours) in the top panel of Figure 2 into correct null forecasts (open circles below the 0.35 contour) in Figure 3; (2) the conversion of the 10 open circles (False Alarms) between the 0.28 and 0.35 PT contours in the top panel of Figure 2 into correct null forecasts (not plotted in Figure 3); and (3) the conversion of one green diamond and one red diamond between the contours in the top plot of Figure 2 into stars, i.e., Missed events, in Figure 3. In a further modification of ESPERTA as applied to ⩾S2 events, alerts are only issued for ⩾M2 flares with data points inside the dashed PT contour lines at the time that the >10 MeV proton flux reaches the S1 (10 pfu) level (i.e., at the end of the third consecutive 5 minute interval with average flux ⩾10 pfu), rather than at SXR peak time plus 10 minutes. This change has the immediate advantage that 21 ⩾ M2 events that triggered forecasts that were S1 FAs (open circles above the contour lines; using 0.35 for the top panel) in Figure 2 are discarded in Figure 3; no ⩾S2 forecast will be made. This gain is partially offset by the corresponding conversion of the 12 blue diamonds above these probability contours in Figure 2 to potential FAs in Figure 3. For all 12 of these events, the SXR peak occurred when the >10 MeV background was <10 pfu. Examination of

[9] The base numbers for the percentages are slightly different from those given in Table 7 of Alberti et al. (2017) because of the net effect of (1) the addition of four FAs to the statistics of Laurenza et al. (2009) by the lowering of the PT for eastern SPEs by Alberti et al. (2017); (2) the correction/conversion of two FAs (2006 December 14 and 2012 July 19) to Hits; (3) the correction/conversion of two mislabeled FAs in Alberti et al. (2017) to correct nulls; and (4) the conversion of an event (2002 August 24, 01:11 UT) not considered in Laurenza et al. (2009) because of a small radio calibration gap to a Hit.

these 12 events reveals that several had relatively long delays to S1 crossing in comparison with the Hits in Table 2. Thus we restricted S2 alerts for such events to those with S1 crossings that followed ⩾M2 SXR peaks within 6/15/30 hr for west/central/eastern flares, respectively. These times correspond to the maximum S1 crossing delays for the 41 Hit events in Table 2. This restriction resulted in the classification of five potential FA events (1998 May 9, W100; 1999 May 3, E32; 2000 June 6, E15; 2002 July 20, E100; 2011 September 22, E74) and one potential Hit (2003 May 28, W21),[10] as correct nulls. As special cases, 11 ⩾ M2 flares with data points inside the dashed PT contour in the three panels in Figure 3 occurred when the background >10 MeV proton flux was ⩾10 pfu. For 5 of these 11 cases (indicated by an * in Table 3) the S2 threshold was not subsequently reached, resulting in FAs. For the six cases, where the >10 MeV flux did reach 100 pfu (indicated by ** in Table 2) the listed WT is the difference between the S2 crossing and the SXR peak time plus 10 minutes. A list of FAs for ⩾S2 SPEs is given in Table 3.

In other departures from the version of ESPERTA applied to S1 events (1) warnings are not issued for ⩾M2 flares when the preflare >10 MeV flux is above the 100 pfu prediction threshold (seven cases), and (2) events that reach the S2 prediction threshold as the result of a delayed shock spike, are counted as Hits or Misses. Delayed shock peaks for ⩾S1 SPEs were considered to be unpredictable by ESPERTA by Laurenza et al. (2009) and Alberti et al. (2017) and the Forecast Result for an associated flare was either listed as a correct null (for data points outside of the PT contours in Figure 2) or an FA (inside the contours). Here, because of the higher S2 prediction threshold and radiation hazard, we attempt to predict such events and identify shock-peak[11] SPEs as Hits or Misses. There are two such SPEs in the sample: No. 59 (a Hit) and No. 35 (Miss; Lario et al. 2008).

The net result of these various modifications associated with the application of ESPERTA to ⩾S2 SPEs for 1995–2014 (Figure 3) is a significant improvement of forecast statistics over those obtained for classical ESPERTA for ⩾S1 events:

1. POD = Hits/(Hits + Misses + MISSES) = 41/(41 + 8 + 6) = 75%.
2. FAR = FAs/(Hits + False Alarms) = 13/(41 + 13) = 24%.

Figure 4 contains the decision tree for making the ESPERTA forecast for ⩾S2 SPE events. The numbers of events involved at each step of the process for the 1995–2014 interval are given in parentheses.

The distribution of WTs for the 41 hits for ⩾S2 SPEs in our sample is shown in Figure 5. The median WT (column 12 in Table 2) is ∼1.7 hr with a minimum WT of ∼0.2 hr. Five events (Nos. 25, 43, 45, 58, and 59, in Table 2) had delays ranging from ∼19 to 65 hr. The associated longitude range of the eruptions was E89-W06. For four of these cases, the

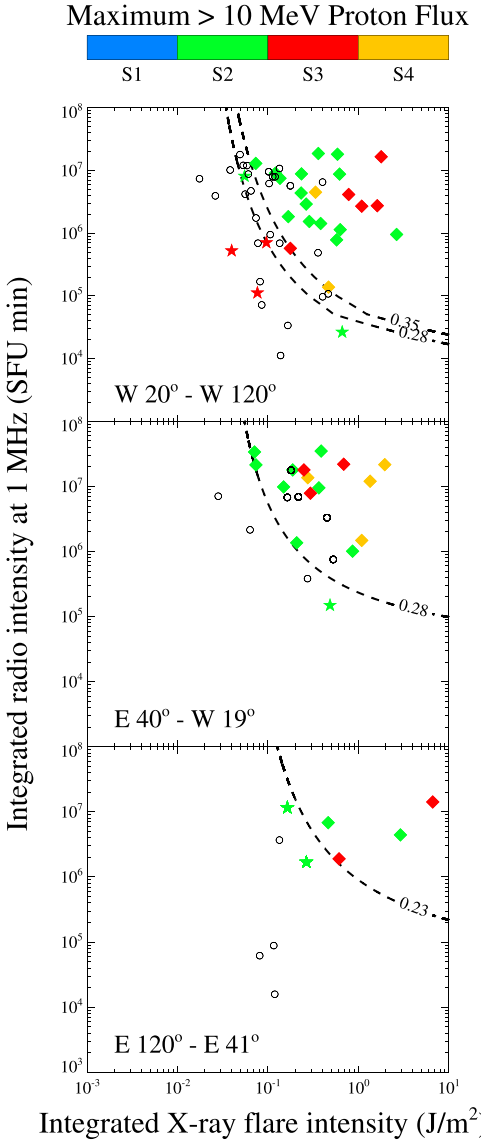

Figure 3. ESPERTA probability contours for prediction of ⩾S2 SPEs for three solar longitude bands. Symbols: open circles outside or between contours—correct null forecasts that were blue stars in Figure 2 or blue diamonds between the 0.28 and 0.35 contours in the top panel of Figure 2; open circles inside (inner) contours—False Alarms; stars—⩾S2 SPEs not predicted (Misses); diamonds—correctly predicted ⩾S2 SPEs (Hits); ⩾S2 SPEs not preceded by ⩾M2 flares—MISSES (not plotted). Color coding gives the NOAA Radiation Storms scale (Table 1).

>10 MeV intensity rose gradually from the S1 threshold to the S2 threshold (see Figure 1). For the fifth case (No. 59), the ⩾100 pfu threshold was reached via a shock spike superimposed on the SPE event.

4. Summary and Conclusion

We applied a modified ESPERTA (Laurenza et al. 2007; Alberti et al. 2017) SPE alert method, previously used only for the ⩾S1 events (with peak >10 MeV proton intensity ⩾10 pfu) typically addressed by such techniques, to the more geoeffective ⩾S2 events (Table 2), which have a >10 MeV flux threshold of 100 pfu. Our model is currently the only validated forecasting technique providing alerts for the enhanced radiation storm level, being relevant for manned space missions. For the 1995–2014 interval, the POD for ⩾S2 events was 75% versus 63% for ⩾S1 events and the FAR was 24% versus 38%. Larger and more

[10] For event No. 29, the responsible flare was an event on May 28 with an SXR peak at 00:27 UT for which the delay to 10 pfu crossing was greater than six hours, precluding a ⩾S2 forecast. The >10 MeV proton flux associated with the flare on the 28th had a delayed shock peak that reached the S2 level at ∼15 UT on the 29th. Thus the ESPERTA S2 forecast for this flare would have been classified as a Miss except for the listed flare that triggered a ⩾S2 alert early on the 29th because the >10 MeV background was greater than 10 pfu. As a result, the flare on May 28 is formally classified as a correct null and the flare on May 29 as a Hit.

[11] Short-term advance warning of shock spikes may also be possible based on satellite observations at L1 (Cohen et al. 2001).

Table 3
False Alarms for ⩾S2 SPEs (1995–2014)

Event Number	SXR Date[a]	SXR Peak Time (hh:mm)	SXR Class	Hα Location	SXR Fluence ($J\ m^{-2}$)	SXR Flag	Radio Fluence (sfu × min)	Radio Frequency (kHz)
1	2000 Jun 10	17:00	M5	N22W39	1.02e–1	5	9.57e+6	940
2	2000 Jul 19*	07:24	M6	S18E10	2.17e–1	2	6.89e+6	940
3	2000 Nov 24	15:13	X2	N21W08	1.64e–1	5	6.77e+6	940
4	2001 Apr 6	19:21	X6	S12E31	4.50e–1	5	3.31e+6	940
5	2001 Apr 12*	10:28	X2	S19W43	4.02e–1	5	6.54e+6	940
6	2001 Oct 22	15:08	M7	S17E19	1.89e–1	5	1.77e+7	940
7	2001 Dec 29*	09:45	X1	S07W85	1.34e–1	1	1.08e+7	940
8	2003 May 31	02:24	X1	S07W65	1.20e–1	5	7.96e+6	940
9	2004 Nov 9*	17:19	M9	N07W51	1.03e–1	5	6.21e+6	940
10	2011 Aug 9	08:05	X6	N17W83	1.77e–1	7	5.71e+6	916
11	2012 Jul 12	16:49	X1	S16W09	5.28e–1	3	7.54e+5	916
12	2012 Jul 19*	05:58	M7	N03W58	3.58e–1	7	4.88e+5	916
13	2014 Apr 18	13:03	M7	S16W41	1.13e–1	5	7.98e+6	916

Note.
[a] Events for which the >10 MeV proton flux was ⩾10 pfu at the peak of the SXR event are indicated with *.

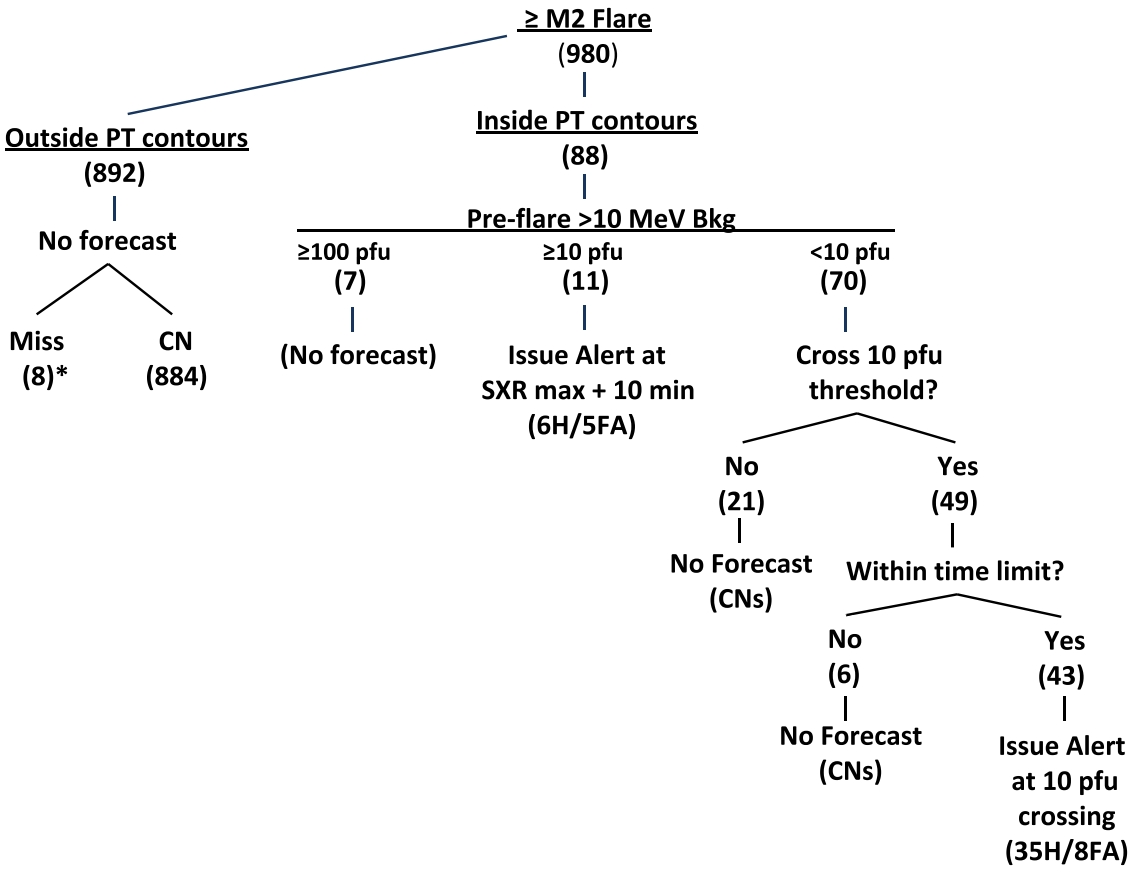

Figure 4. Decision tree for ESPERTA forecasts of ⩾S2 SPEs (1995–2014). PT—prediction threshold; CN—correct null; H—Hit; FA—False Alarm. The symbol * indicates that there are six other misses (MISSes in Table 2) from visible disk flares that did not reach the M2 level. Four other ⩾S2 events were associated with <M2 flares from behind the solar limb.

hazardous SEPs are somewhat easier to forecast than the classic ⩾S1 events.

The improvement in the POD and FAR parameters appears to result from a beneficial effect of the big flare sydrome (BFS; Kahler 1982). From 1995 to 2014, CMEs associated with ⩾S1 events had a median speed of 1289 $km\ s^{-1}$ (similar to that reported in Gopalswamy 2010a) versus a corresponding value of 1743 $km\ s^{-1}$ for ⩾S2 events. CME kinetic energy is the dominant component in the energy budget of eruptive flares (Emslie et al. 2012). As another indication of the BFS effect, all 14 of the ground level enhancements (GLEs; detected by neutron monitors and due to SEP events with acceleration of protons to >500 MeV) from 1995 to 2014, for which an ESPERTA ⩾S2 forecast would have been made, are Hits in

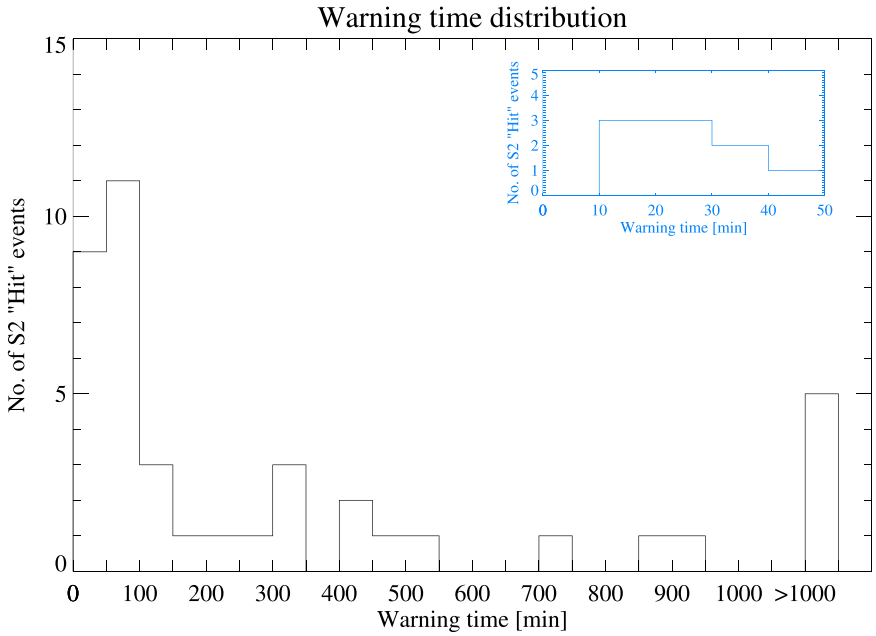

Figure 5. Histogram of warning times for ESPERTA predictions of ⩾S2 >10 MeV proton events. Inset for predicted SPEs with warning times ⩽50 minutes.

Table 2 (see Souvatzoglou et al. 2014, their Table 4). No forecasts were made for three GLEs because the associated flare was <M2 and located behind the solar limb (2001 April 18) or because the >10 MeV flux was >100 pfu at the time of the associated flare (2003 October 29 and 2005 January 17).

Normally, the BFS is viewed as a hindrance that makes it difficult to decipher the physics of big flares. For the SPE alert application, however, delaying the forecast of a ⩾S2 event until the S1 level is reached (which applies in the bulk of the cases, 35 of 41 Hits) provides important new information for the ESPERTA technique as we are now considering flares with a demonstrated potential to produce base-level SPE impacts, a qualitative input that supplements the consideration of big flares (i.e., large SXR and ∼1 MHz fluences) in the application of ESPERTA to ⩾S2 events. ESPERTA employs ∼1 MHz radio fluence as evidence of escaping particles assuming that the low-energy (∼5 keV; Cliver & Ling 2009) electrons responsible for this emission are accompanied by >10 MeV protons. In the application of ESPERTA to ⩾S2 events, the presence of such protons is specifically required by withholding a forecast until the S1 threshold is reached. The value of this new information is apparent in the high Hit/FA ratio (35/8) in Figure 4 for SPEs that have crossed the S1 threshold. If, generally, the BFS means that big flares have more of everything (e.g., greater SXR peak intensities, faster CMEs), then a selection of even more energetic events is more likely to have the attribute of ⩾S2 SPE association.

Looking ahead, delayed forecasts of ⩾S2 events allow more time following solar eruptions to refine the estimated flare SXR and radio inputs currently used for longer-duration flares in ESPERTA and other empirical models. Alternatively, it permits the possibility to use inputs that are thought to be more directly related to the proton acceleration process in eruptive flares (e.g., CME speed and DH type II burst association; Cliver 2004; Gopalswamy 2010b; St. Cyr et al. 2017) in addition to, or in lieu of, the more flare-based parameters currently used by ESPERTA.

We thank Ian Richardson for sharing results in advance of publication. All data used in this analysis are publicly accessible from NASA (*Wind*/WAVES) and NOAA (*GOES*). The *Wind*/WAVES data were obtained from ftp://solar-radio.gsfc.nasa.gov/. *GOES* data have been downloaded from the http://www.ngdc.noaa.gov/stp/satellite/goes/dataaccess.html repository.

ORCID iDs

M. Laurenza https://orcid.org/0000-0001-5481-4534
T. Alberti https://orcid.org/0000-0001-6096-0220
E. W. Cliver https://orcid.org/0000-0002-4342-6728

References

Alberti, T., Laurenza, M., Cliver, E. W., et al. 2017, ApJ, 838, 59
Anastasiadis, A., Papaioannou, A., Sandberg, I., et al. 2017, SoPh, 292, 134
Balch, C. C. 2008, SpWea, 6, S01001
Barnes, G., Leka, K. D., Schrijver, C. J., et al. 2016, ApJ, 829, 89
Bougeret, J. L., Kaiser, M. L., Kellog, P., et al. 1995, SSRv, 71, 231
Cane, H. V., Richardson, I. G., & von Rosenvinge, T. T. 2010, JGR, 115, A08101
Cliver, E. W. 2016, ApJ, 832, 128
Cliver, E. W., Kahler, S. W., & McIntosh, P. S. 1983, ApJ, 264, 699
Cliver, E. W., Kahler, S. W., & Reames, D. V. 2004, ApJ, 605, 902
Cliver, E. W., & Ling, A. G. 2009, ApJ, 690, 598
Cohen, C. M. S., Mewaldt, R. A., Cummings, A. C., et al. 2001, JGR, 106, 20979
Dierckxsens, M., Tziotziou, K., Dalla, S., et al. 2015, SoPh, 290, 841
Emslie, A. G., Dennis, B. R., Shih, A. Y., et al. 2012, ApJ, 759, 71
Garcia, H. A. 1994, ApJ, 420, 422
Gopalswamy, N. 2010a, in Proc. 20th Nat. Sol. Phys. Meeting, ed. I. Dorotovič (Hurbanovo: Slovak Central Observatory), 108
Gopalswamy, N. 2010b, in Heliophysical Processes, ed. N. Gopalswamy, S. Hasan, & A. Ambastha (Berlin: Springer), 53
Gopalswamy, N., Yashiro, S., Michalek, G., et al. 2009, EM&P, 104, 295
Kahler, S. W. 1982, JGR, 87, 3439
Kahler, S. W., Cliver, E. W., & Ling, A. G. 2007, JASTP, 69, 43
Lario, D., Decker, R. B., Malandraki, O. E., & Lanzerotti, L. J. 2008, JGR, 113, A03105
Laurenza, M., Cliver, E. W., Hewitt, J., et al. 2009, SpWea, 7, S04008

Laurenza, M., Hewitt, J., Cliver, E. W., Storini, M., & Ling, A. 2007, in 20th Eur. Cosmic Ray Symp., Solar Energetic Proton Events and Soft X-ray Flares http://www.lip.pt/events/2006/ecrs/proc/ecrs06-s1-34.pdf
Marubashi, K., Akiyama, S., Yashiro, S., et al. 2015, SoPh, 290, 1371
McCullagh, P., & Nelder, J. A. 1983, Generalized Linear Models (London: Chapman and Hall) 98–155 chap. 4
Núñez, M. 2011, SpWea, 9, S07003
Papaioannou, A., Anastasiadis, A., Sandberg, I., et al. 2015, J. Physics Conference Series, 632, 012075
Papaioannou, A., Sandberg, I., Anastasiadis, A., et al. 2016, JSWSC, 6, A42
Pesnell, W. D. 2012, SoPh, 281, 507
Posner, A. 2007, SpWea, 5, S05001
Reames, D. V. 1999, SSRv, 90, 413
Reames, D. V. 2013, SSRv, 175, 53
Reames, D. V. 2017, Solar Energetic Particles (Heidelberg: Springer)
Richardson, I. G., von Rosenvinge, T. T., Cane, H. V., et al. 2014, SoPh, 289, 3059
Signoretti, F., Laurenza, M., Marcucci, M. F., & Storini, M. 2011, Proc. ICRC (Beijing), 10, 267
Silverman, B. W. 1998, Density Estimation For Statistics and Data Analysis (Boca Raton, FL: CRC Press)
Souvatzoglou, G., Papaioannou, A., Mavromichalaki, H., Dimitroulakos, J., & Sarlanis, C. 2014, SpWea, 12, 633
St. Cyr, O. C., Posner, A., & Burkepile, J. T. 2017, SpWea, 15, 240
Storini, M., Cliver, E. W., Laurenza, M., & Grimani, C. 2008, OPOCE Publisher for COST 724 Action (Luxembourg: OPOCE), 63
Winter, L. M., & Ledbetter, K. 2015, ApJ, 809, 105
Yashiro, S., Gopalswamy, N., Michalek, G., St., et al. 2004, JGR, 109, A07105